J. Electrochem. Sci. Eng. **15(2)** (2025) 2479; http://dx.doi.org/10.5599/jese.2479

Open Access : : ISSN 1847-9286
www.jESE-online.org

Original scientific paper

Ecofriendly synthesis of $NiZnFe_2O_5$ nanoparticle by papaya leaf extract for electrochemical detection of ascorbic acid in orange juice and pharmaceuticals

Gubbihalli Nanjundappa Chandana[1], Murudagalli Basavaraju Shivaswamy[1], Mandya Shivananju Asha[2], Shanthalingaiah Jeevitha[1], Honnegowdanahalli Shivabasappa Nagendra Prasad[1,✉], Bendekere Shankarappa Hemanth[1,4], Madanahalli Ankanathappa Sangamesha[3], Beejaganahalli Sangameshwara Madhukar[1], Lingappa Mallesha[5], Jamballi G. Manjunatha[6]

[1]*Department of Chemistry, Sri Jayachamarajendra College of Engineering, JSS Science and Technology University, Mysuru-570 006, Karnataka, India*
[2]*Department of Studies and Research Centre in Chemistry (A Recognized Research Centre of University of Mysore), St. Philomena's College Bannimantapa, Mysuru 570015, Karnataka, India*
[3]*Department of Chemistry, The National Institute of Engineering, Mysuru-570008, Karnataka, India*
[4]*Centre for Nano and Material Sciences, JAIN (Deemed-to-be University), Jain Global Campus, Kanakapura, Bangalore, Karnataka-562112, India*
[5]*JSS College of Arts, Commerce and Science, Ooty road, Mysuru, Karnataka-570008, India*
[6]*Department of Chemistry, FMKMC College, Constituent College of Mangalore University, Madikeri, Karnataka-571201, India*

Corresponding author: ✉nprasad@jssstuniv.in

Received: August 21, 2024; Accepted: November 30, 2024; Published: December 11, 2024

Abstract

A green technique has been employed to synthesize the $NiZnFe_2O_5$ nanoparticles using papaya leaf extract. The X-ray diffraction investigated the structural characteristics and crystalline size. The morphology of the synthesised nanoparticle is analysed by scanning electron microscopy. The average diameter of the nanoparticle is 47.93 nm, which was determined using the dynamic light scattering method. UV/Vis diffuse reflectance spectrum results revealed that the $NiZnFe_2O_5$ NPs band gap is 1.8 eV. It was calculated using the Kubelka-Monk function and energy dispersion X-ray spectroscopy analysis was used to identify the synthesized nanoparticle's elements. The electrochemical behaviour of $NiZnFe_2O_5$ modified glassy carbon electrode (GCE) and bare GCE was studied to detect ascorbic acid using cyclic voltammetry and differential pulse voltammetry. Compared to unmodified GCE, $NiZnFe_2O_5$ nanoparticles modified GCE exhibit excellent electrocatalytic activity towards the AA oxidation, which was proved by the increase in peak current and decrease in peak potential. Electrochemical impedance analysis suggests that the

NiZnFe2O5 nanoparticles significantly enhance the charge transfer rate. The linear response of the peak current on the concentration of AA was obtained in the range of 0.2-50 µM. The detection limit was found to be 1.038 µM. The present work serves as a systematic benchmark to assess the electrochemical sensing potential of $NiZnFe_2O_5$ NPs towards AA in orange juice and pharmaceuticals.

Keywords
Green synthesis; glassy carbon electrode; cyclic voltammetry; differential pulse voltammetry; vitamin-C tablets

Abbreviations

PLE - Papaya leaf extract
$NiZnFe_2O_5$ NPs - Nickel zinc ferrite oxide nanoparticle
NPs - Nanoparticles
AA - Ascorbic acid
XRD - X-ray powder diffraction
JCPDS - Joint committee on powder diffraction standards
SEM - Scanning electron microscopy
EDX - Energy dispersion X-ray spectroscopy
UV-Vis DRS - Ultraviolet visible diffusion reflectance spectroscopy
DLS - Dynamic light scattering
GCE - Glassy carbon electrode
EIS - Electron impedance spectroscopy
CV - Cyclic voltammetry
DPV -Differential pulse voltammetry
R_{ct} - Charge transfer resistance
I_{pa} - Anodic peak current
LOD - Limit of detection

Introduction

Nanoparticles are synthesised due to their unique properties and are applied to various fields such as biomedical, materials science, and environmental treatment. Compared to other techniques of nanoparticle synthesis [1], green synthesis, which uses naturally occurring sources such as plant extracts, algae, bacteria, and fungi, is more affordable, scalable, and environmentally friendly. The natural product has abundant bioactive properties that help stabilize and reduce nanoparticles during synthesis. *Carica* papaya leaf extract acts as a stabilizing and reducing agent due to the presence of flavonoids like quercetin and kaempferol, which help reduce metal ions to their nano size [2]. Papain and other alkaloids have chelating qualities that stabilize the nanoparticles by preventing agglomeration. Further aiding in the manufacturing process are additional bioactive substances, including phenolic acids and terpenoids, which supply functional groups for encasing the nanoparticles. *Carica* papaya leaf extract is also a great option for green synthesis because of its many benefits, which include biocompatibility, cost-effectiveness and availability.

Ferrites are generally understood to be ferromagnetic compounds made up of iron oxides. Nevertheless, they can also be chemically combined with other metals to give them magnetic and dielectric qualities. Within this category, spinel ferrites have been used in sensors recently because of their distinct qualities, including their high reactivity, high specific area, environmental friendliness, insensitivity to moisture, and scalability [3]. In the ultra-thin form, nickel ferrites ($NiFe_2O_4$) display a non-collinear spin structure and an inverted spinel structure varying with ferromagnetic and superparamagnetic properties of ferrites having a significant influence. It finds use in the medical domain,

including magnetic resonance imaging, medication delivery, and cancer therapies. They also have applications in electronics, including sensors, telecommunications, catalysts and high-frequency transformers [4].

The iron(III) oxide nanocomposite and reduced graphene oxide modified GCE are used to detect AA electrochemically [5,6]. L-ascorbic acid (AA) is a water-soluble vitamin with strong antioxidant properties that neutralizes harmful free radicals. The human body can only get the necessary amount of ascorbic acid from outside sources, unlike plants and the majority of animals that can synthesise AA from glucose [7]. Real samples such as orange juice, AA pills, avocado pear, garlic, green beans and cucumber contain AA. However, there may be health consequences from excessive or insufficient ingestion, which is why accurate detection techniques are important concerning their sensitivity, affordability, ease of use and possibility for real-time monitoring, electrochemical sensors present a promising method for the sensitive and selective detection of ascorbic acid. This work describes a straightforward electrochemical sensor production method that modified GCE to enable the sensing and targeted detects AA using $NiZnFe_2O_5$ NPs. It is important to note that the work also represents electrochemical detection in real samples such as orange juice and vitamin C tablets.

Experimental

Chemicals and reagents

Nickel nitrate ($Ni(NO_2)_2$), zinc nitrate ($Zn(NO_2)_2$), ferric nitrate ($Fe(NO_2)_3$), potassium chloride (KCl), ascorbic acid, ethylene glycol ($C_6H_8O_2$) and liquid ammonia were purchased from Sigma Aldrich chemical industries, Bengaluru, Karnataka, India and these compounds were used without any further purification in the experiment.

Extraction procedure

The *carica* papaya leaves of red leady bread were collected from the garden located in Bogadi, Mysuru, Karnataka, India. The leaves were initially washed two times with tap water, then washed with deionized water and ethanol wash to remove certain pests, steam from the leaf, and dried for 15 days, then blended to make a powder. 20 g of leaf powder was taken in a 250 ml beaker and 30 ml of deionized water was added with a constant stirring at a temperature of 80 °C for 2 hours. Cool the mixture at room temperature, then filter the mixture using a clean muslin cloth by a hand-pressing method and collect the filtrate. The obtained filtrate is PLE, which is further used as a fuel for nanoparticle synthesis.

Synthesis of nickel zinc ferrite ($NiZnFe_2O_5$) nanoparticles

$NiZnFe_2O_5$ NPs were synthesized using the solution combustion method. Nickel nitrate ($Ni(NO_2)_2$), zinc nitrate ($Zn(NO_2)_2$), and ferric nitrite ($Fe(NO_2)_3$) are used as precursor materials and PLE as a reducing agent. Stoichiometrically weighed 0.025 M zinc nitrite ($Zn(NO_2)_2$) and 0.05 M ferric nitrite ($Fe(NO_2)_3$) were taken in a 250 ml beaker containing 50 ml of ethylene glycol and continuously stirred for about 30 minutes. Then, stoichiometrically calculated 0.025 M nickel nitrate ($Ni(NO_2)_2$) was slowly added to the above solution, followed by adding 5 ml of PLE. Further, 1 ml of liquid NH_3 was periodically added during the synthesis to maintain the pH between 7 and 8. The mixture is stirred and heated at 50 °C for 3 hours to obtain a gel. Then, the calcination is carried out using a muffle furnace at a temperature of 600 °C for 4 hours. Similarly, the other two sets of solutions are prepared using 10 ml and 15 ml PLE. Eco-friendly synthesized nanoparticles are confirmed by different characterization techniques and used for electrochemical applications [8].

Characterization of nickel zinc ferrite ($NiZnFe_2O_5$) nanoparticles

The XRD (3proto A - XRD equipped with Cu Kα radiation λ = 0.15406 nm, Mysuru) is utilized to determine the crystal structure and crystallite size of materials of the synthesized nanoparticle. The SEM (VEGA3 TESCAN, Brno, Czech Republic, Bangalore) is employed in the morphological investigation and surface features of $NiZnFe_2O_5$ nanoparticles. It provides high-resolution images, allowing us to observe the shape and surface structure of the nanoparticles. EDX (SWIFT 3000 SDD DETECTOR, Mysuru) is employed to determine the material's elemental composition. It provides quantitative evidence regarding the fundamental composition present in the sample, verifying the presence of specific elements and assessing their uniform distribution of elements within the nanoparticles. UV-Vis diffuse reflectance spectroscopy (PE Lambda20 Spectroscopy, Mysuru) is utilized to measure the absorption, reflectance and optical properties of the nanoparticle. The Malvern Zeta sizer Nano ZS-90 (Malvern Instruments, Mysuru) was used to estimate particle size along with size distributions in aqueous or physiological solutions at 25 °C. A CHI 608D electro-chemical analyser was used to work on the electrochemical sensor.

Electrochemical sensors

The electrochemical sensor activity of synthesized $NiZnFe_2O_5$ NPs was investigated using a computer-controlled CHI 608D analyser. The CHI instrument is made up of three electrode systems:

1) reference electrode (silver-silver chloride electrode),
2) counter electrode (platinum electrode), and
3) working electrode (glassy carbon electrode).

Working electrode surfaces were polished with different sizes of alumina powder (0.3, 0.1 and 0.05 µm) and rinsed with deionized water. Synthesized $NiZnFe_2O_5$ NPs (1 mg) were sonicated in water and ethanol for 20 to 30 minutes until fully dispersed. Then, the working electrode surface was drop cast with dispersed $NiZnFe_2O_5$ NPs, which were allowed to dry at room temperature. The modified electrode was used for electrochemical sensors.

Real sample preparation

The orange fruits were obtained at the local market and peeled the covering and squeezed completely. The collected orange juice samples were transferred into a 250 ml beaker. The tablets were brought from nearby medical shops, crushed using a mortar, and transferred to a 250 ml beaker containing deionized water. Then, the sample was centrifuged for further analysis.

Results and discussion

X-ray diffraction

XRD patterns are used to examine the crystallinity of the $NiZnFe_2O_5$ NPs. Figure 1 displays the XRD analysis of $NiZnFe_2O_5$ NPs. The peaks appearing at 2θ = 31.83, 56.63 and 70.05° were corresponded to Zn (100), Zn (110), and Zn (201) planes, respectively (JCPDS Card No. 22-1012) [9]. Peaks appearing at 2θ = 30.15, 35.56, 43.20, 53.43, 57.03 and 62.65°, these correspond to Fe (220), Fe (311), Fe (400), Fe (422), Fe (511) and Fe (440) planes respectively (JCPDS Card No.10-0325). Peaks appearing at 2θ = 37.02, 62.65 and 74.11° correspond to Ni (111), Ni (220), and Ni (311) and are coordinated with a JCPDS Card No. 10-0325 [10].

A comparison of the XRD patterns of the synthesized nanoparticle revealed that the peaks associated with the $NiZnFe_2O_5$ NPs are sharpened with an increase in the volume of PLE in the synthesised samples [11].

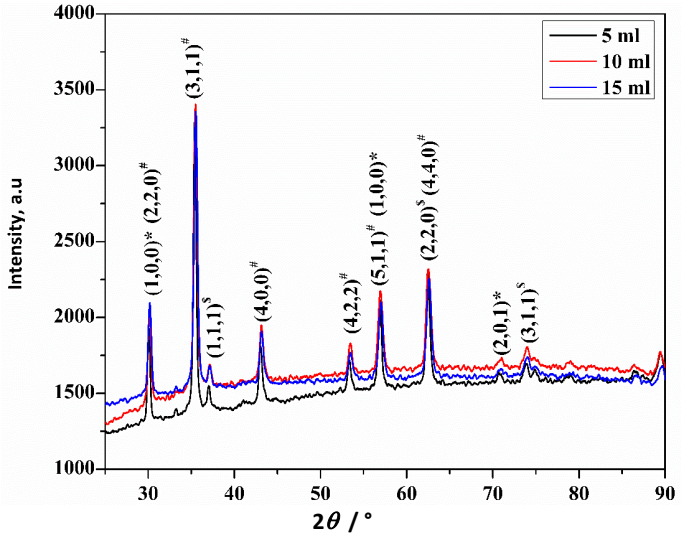

Figure 1. *XRD spectra of $NiZnFe_2O_5$ NPs synthesised using three different volumes of PLE, 5, 10 and 15 ml (*, #, $, indicate Zn, Fe, Ni, respectively)*

The obtained peaks are narrow, which suggests that the synthesized $NiZnFe_2O_5$ NPs are crystalline. The crystalline size of synthesized $NiZnFe_2O_5$ NPs is calculated by Debye-Scherrer's length formula, Equation (1):

$$D = \frac{0.94\lambda}{\beta \cos\theta} \quad (1)$$

where λ is the wavelength of the X-ray radiation, β is the full-width at half maximum (FWHM) of the strongest intensity diffraction peak, θ is the angle of the strongest characteristic peak, and D is the average crystallite size. From Debye-Scherrer's length equation at the plane (311), the size of synthesized $NiZnFe_2O_5$ NPs ranges from 55 to 59 nm. Calculated data is given in Table 1.

Table 1. *XRD data of synthesized $NiZnFe_2O_5$ NPs (311) plane*

Volume of PLE added, mL	β	2θ / °	Scherrer's length, nm
5	0.2542	35.56	59.8
10	0.2655	35.56	57.2
15	0.2724	35.56	55.7

Scanning electron microscopy and energy-dispersive X-ray spectroscopy

The development of $NiZnFe_2O_5$ NPs was analysed *via* SEM and EDX, as shown in Figure 2 (A, B, C). The effect of PLE volume used in the synthesis of $NiZnFe_2O_5$ NPs is noticeable. The synthesized $NiZnFe_2O_5$ NPs present different shapes and are regular in size, with increased use of PLE in the synthesis process. EDX analysis shows that elements are evenly distributed across three samples. The nanoparticle surface exhibits the excellent distribution of nickel, zinc, iron, and oxygen with 9.78, 18.70, 56.10,15.43 wt.% for 5 mL of PLE added; 9.24, 18.13, 48.40, 28.81 wt.% for 10 mL of PLE added and 8.06, 16.30, 46.84, 24.22 wt.% for 15 mL of PLE added. The synthesized nanoparticles have high purity and no interference [12].

UV-vis diffuse reflectance spectroscopy

The diffuse reflectance spectra of $NiZnFe_2O_5$ NPs were displayed in Figure 3 and the band gap of the synthesized nanoparticle was calculated using Kubelka-Munk Equation (2).

$$F(R_\infty) = (1-R_\infty^2)/2R_\infty = K/S \quad (2)$$

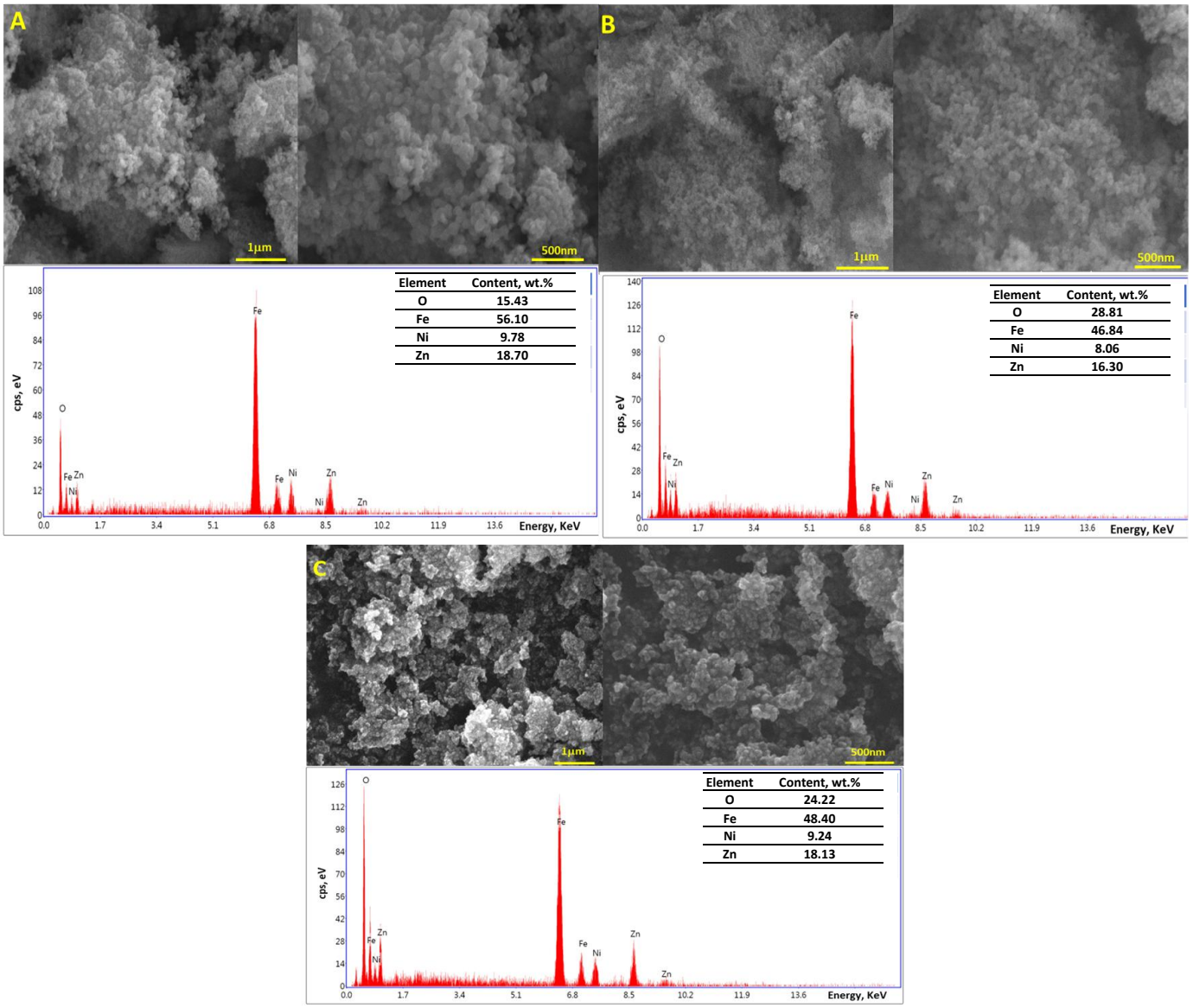

Figure 2. *SEM images and EDX analysis of synthesized $NiZnFe_2O_5$ NPs for A) 5; B) 10 and C) 15 ml of PLE added*

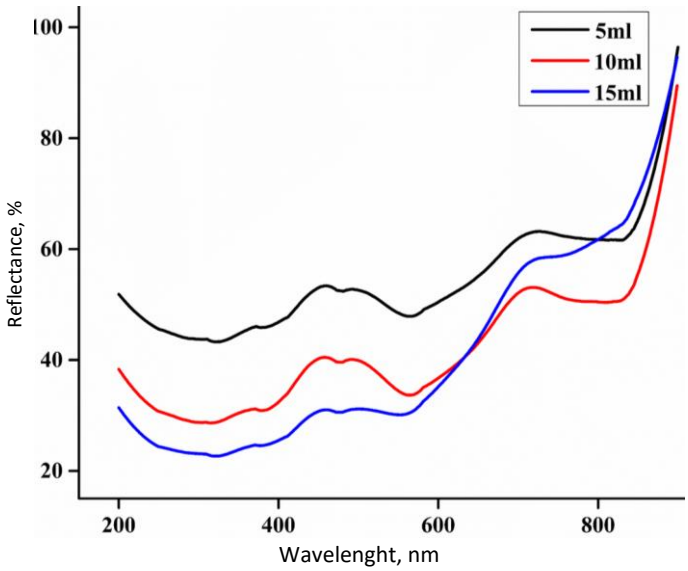

Figure 3. *UV-vis diffuse reflectance spectroscopy of synthesized $NiZnFe_2O_5$ NPs with different volumes of PLE*

with $F(R_\infty)$ being the Kubelka-Munk function and R_∞ being the diffuse reflectance of the nanoparticle, K is the absorption coefficient, and S is the scattering coefficient.

The result demonstrated that the band gap of $NiZnFe_2O_5$ NPs is about 1.8 eV. According to the literature, the calculated band gap of 1.8 eV was acceptable for catalytical activity for electrochemical sensor analysis [13].

Dynamic light scattering

Dynamic light scattering was used to determine the particle size. Figure 4 indicates the average crystalline size of 47.93 nm was obtained from a highly dispersed mixture in this experiment. $NiZnFe_2O_5$ NPs show more stability in aqueous solutions, as indicated by the polydispersity index (PDI), which was 0.633. These values are consistent with the Scherer's length calculation from the XRD investigation [14]. This relates to the manufactured $NiZnFe_2O_5$ NPs with 15 ml of PLE, a nanoscale composition.

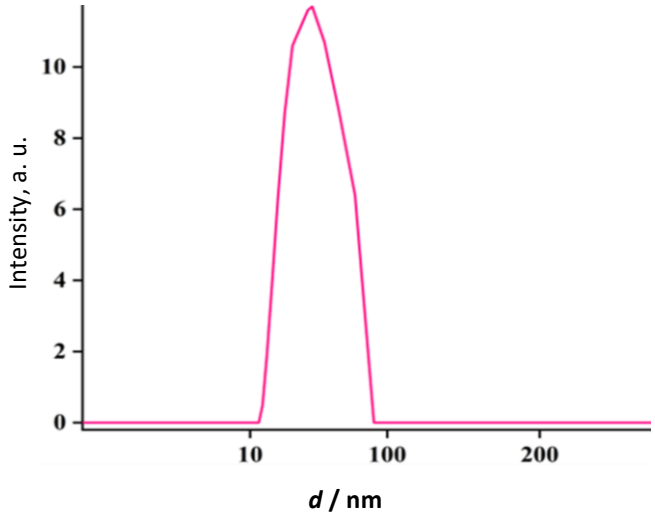

Figure 4. *Dynamic light scattering (DLS) of synthesized $NiZnFe_2O_5$ NPs with a volume of PLE 15 ml*

Electrochemical performance of $NiZnFe_2O_5$/GCE NPs

The electrochemical analysis of bare GCE and $NiZnFe_2O_5$ NPs/GCE modified electrodes were examined by CV in 0.1 M KCl (pH 7) with a scan rate of 0.5 V/s in the potential range of -1.4 to +1.4 V. Figure 5A represents the cyclic voltammograms of bare GCE and $NiZnFe_2O_5$/GCE NPs in the absence of an analyte. Bare GCE and $NiZnFe_2O_5$ NPs/GCE do not exhibit any current peak. The bare GCE and $NiZnFe_2O_5$ NPs/GCE electrodes were analysed using electrochemical impedance spectroscopy (EIS) and CV to investigate surface modifications. In Figure 5B, a redox peak appears due to the presence of $[Fe(CN)_6]^{3-/4-}$ at a potential 0.42 V and 0.13 V, which confirms the modified $NiZnFe_2O_5$ NPs/GCE shows a higher peak current compared to bare GCE. According to Equation (3), the modified electrode has a greater surface area than the bare GCE at room temperature of 25 °C.

$$I_{pa} = (2.69 \times 10^5)\, n^{3/2}\, AC(Dv)^{1/2} \quad (3)$$

In Equation (3) I_{pa} is the peak anodic current of the analyte, A is the electrochemically active surface area, n is the number of electrons, C is the analyte concentration, v is the scan rate and D is the diffusion coefficient of the analyte. The calculated electrochemical active area of $NiZnFe_2O_5$ NPs/GCE and GCE are 0.51685 and 0.243955 cm^2, respectively. The results show that $NiZnFe_2O_5$ NPs/GCE has approximately 2.12 times greater active surface area than GCE. Thus, $NiZnFe_2O_5$ NPs/GCE has much better electrochemical sensing properties than GCE [15,16].

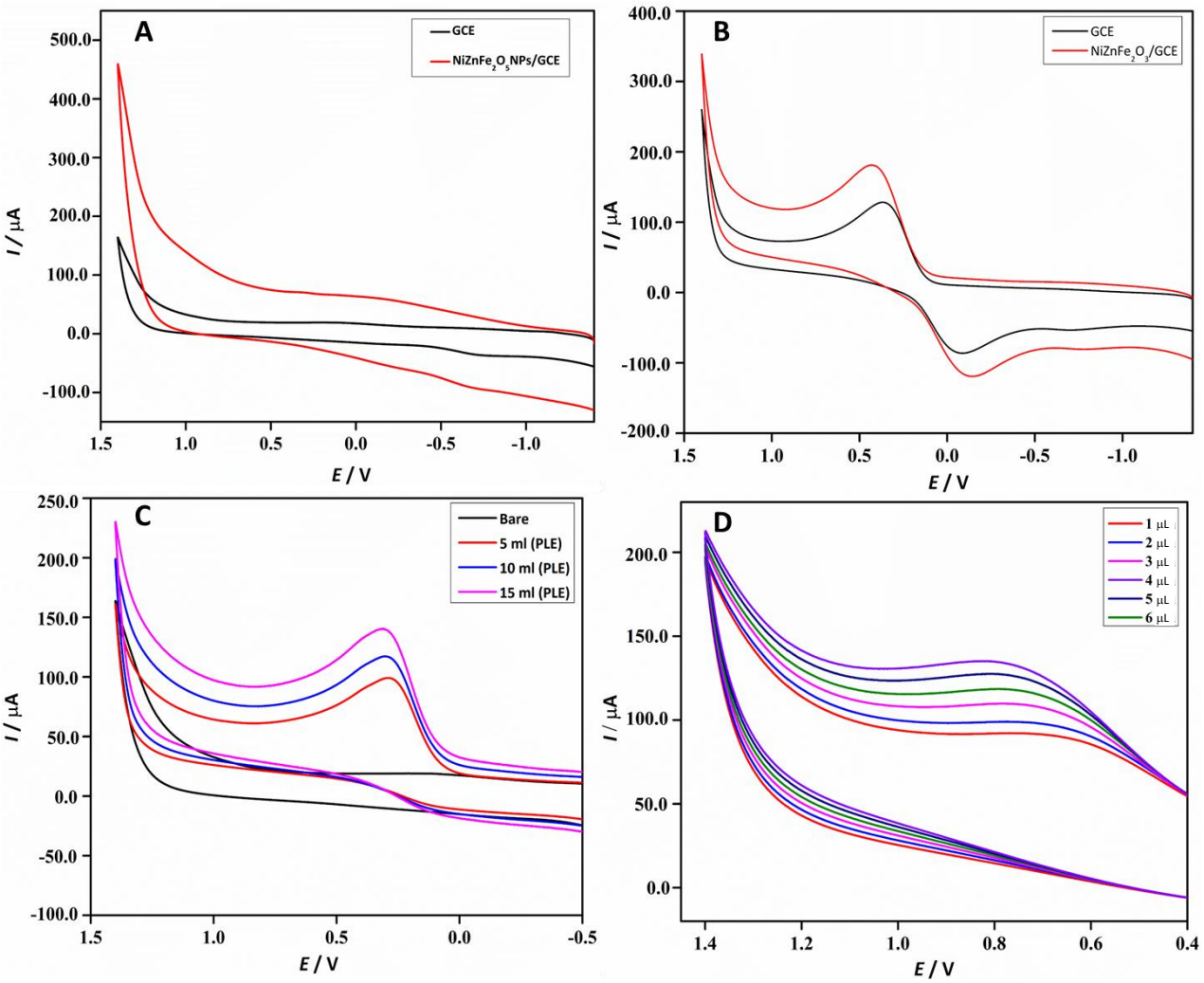

Figure 5. *Cyclic voltammetry (0.5 V s^{-1}) of bare GCE and $NiZnFe_2O_5$ NPs/GCE in 0.1 M KCl: A) in the absence of analyte; B) in the presence of 3 mM $[Fe(CN)_6]^{3-/4-}$; C) with 2.5 µM AA different volumes of PLE added; D) CV responses of $NiZnFe_2O_5$ NPs/GCE in 0.1 M KCl with 2.5 µM AA for different drop-casting volumes of $NiZnFe_2O$ NPs*

In comparison to the bare GCE, the $NiZnFe_2O_5$ NPs/GCE modified electrode synthesized using different PLEs exhibits a substantially greater CV response. This enhanced performance is caused by the presence of $NiZnFe_2O_5$ NPs. Three distinct NPs with varying volumes of PLE and sensing capabilities exhibit responsiveness to a 2.5 µM AA dose. Figure 5C clearly shows the high peak current for $NiZnFe_2O_5$ NPs synthesized using 15 ml of PLE.

The I_{pa} increases with the drop-casting volume in the range from 1.0 to 4.0 µL. However, after 5.0 µL, the I_{pa} gradually decreases with an increase in $NiZnFe_2O_5$ NPs concentration (Figure 5D). This is due to the increased resistance on GCE at higher drop-casting volumes. Thus, 4.0 µL was used for drop-casting $NiZnFe_2O_5$ NPs modified GCE for further electrochemical investigations.

Electrochemical impedance spectroscopy

EIS is a widely used analytical technique for analysing the interfacial properties of the modified electrode's surface. The electron transfer characteristics of the electrode interface in 3.0 mM of $[Fe(CN)_6]^{3-/4-}$ with 0.1 M KCl and a scan rate of 0.5 V/s were examined using CV and EIS techniques. Based on the Nyquist plot, measured EIS spectra of the bare GCE and $NiZnFe_2O_5$NPs/GCE are displayed in Figure 6. Randles equivalent circuit in Figure 6 gives the R_{ct} values of 148.1 and 84.44 Ω for bare/GCE and $NiZnFe_2O_5$NPs/GCE, respectively.

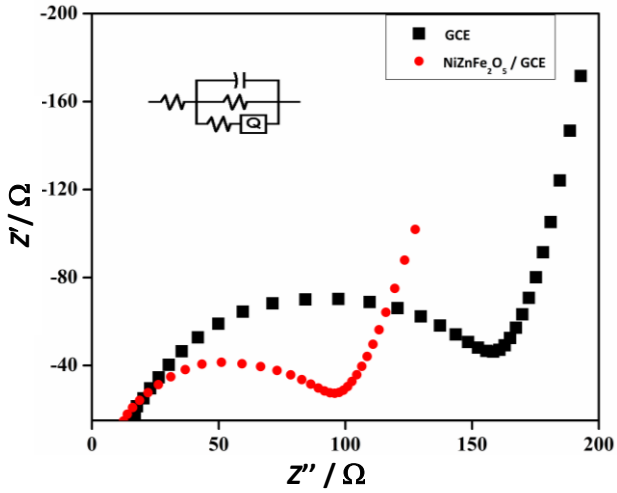

Figure 6. *Impedance spectra of bare GCE and $NiZnFe_2O_5$ NPs/GCE in 0.1M KCl with 3 mM $[Fe(CN)_6]^{3-/4-}$ and Randles equivalent circuit (insert)*

Effect of scan rate

The electrocatalytic properties of $NiZnFe_2O_5$ NPs/GCE-modified electrodes were evaluated using CV in the presence of AA. CV was measured using 2.5 µM AA in 0.1 M KCl (pH 7) with different scan rates from 0.25 to 2.0 V/s. Figure 7A indicates the increase in the peak current with the increase in the scan rate.

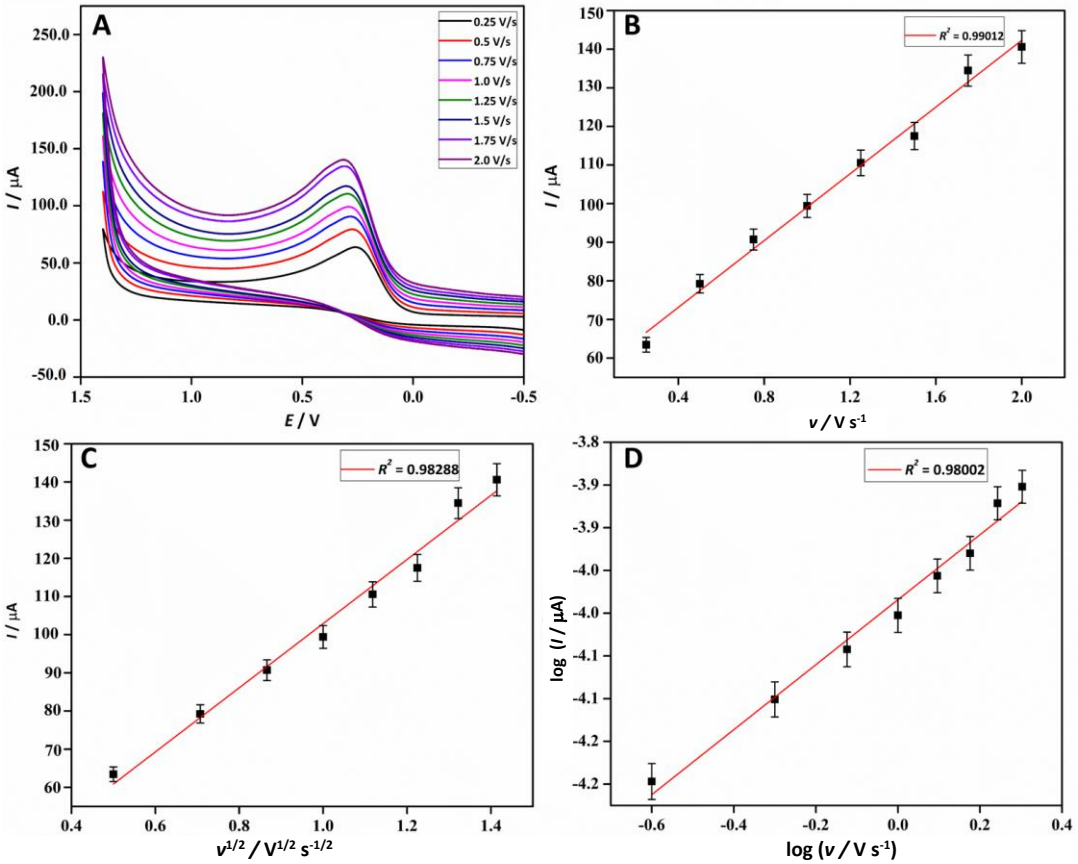

Figure 7. *A) Cyclic voltammetry of $NiZnFe_2O_5$ NPs/GCE of 0.1 M KCl (pH 7) with 25µM AA by varying the scan rates, B) anodic peak current vs. scan rate, C) anodic peak current vs. square root of scan rate. D) anodic peak of log of anodic peak current* vs. *log of scan rate*

Figure 7B shows a linear relationship between peak current *vs*. scan rate. According to Equation (4), the obtained regression coefficient value is 0.99012 (I_{pa}). Scan rate tests were conducted to

determine whether the process occurring on the surface of $NiZnFe_2O_5$NPs/GCE is diffusion-controlled or controlled by adsorption. Figure 7C indicates the direct correlation between the square root of the scan rate *vs*. peak current and from Equation (5), the exhibited correlation coefficient R^2 is 0.9828. A plot of the logarithm of scan rate *vs.* logarithm of scan rate peak current (Figure 7D) results in a straight line with a slope of 0.3814 in Equation (6). The obtained value of 0.3814 is near the theoretical value of 0.5 for a directly diffusion-driven process [17,18].

$$I_{pa} = 4.32266\times10^{-5}\, v + 5.58643\times10^{-5}\ (R^2 = 0.99012) \quad (4)$$

$$I_{pa} = 8.40129\ v^{1/2} + 1.88862\ (R^2 = 0.98288) \quad (5)$$

$$\log I_{pa} = 0.38014 \log v - 3.98423\ (R^2 = 0.98002) \quad (6)$$

Effect of ascorbic acid concentrations

The electrochemical behaviour of the modified electrode was examined by varying the analyte concentration from 0.8 to 6.2 µM at a scan rate of 0.5 V/s. The peak current linearly increases with the increase in the concentration of AA from 0.8 to 6.2 µM, as shown in Figure 8A. According to the data, $NiZnFe_2O_5$ NPs/GCE electrode acts as electrocatalysts for the electrochemical detection of AA. Figure 8B shows the calibration plot of current *vs.* concentration. It gives a linear relationship between concentration and current, and the regression coefficient value calculated using Equation (7) is 0.99592.

$$I_{pa} = 1.52853\times10^{-4}\, C_{AA} + 5.57913\times10^{-5}\ (R^2 = 0.99592) \quad (7)$$

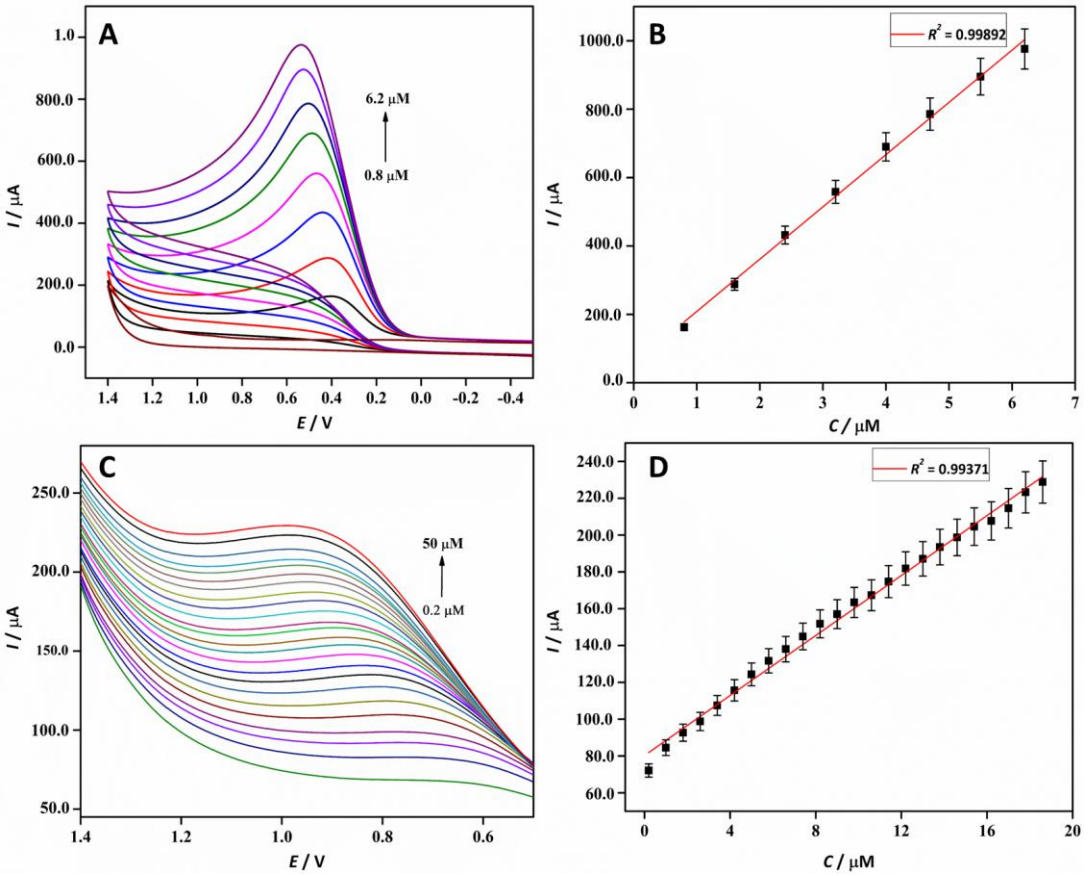

Figure 8. *A) Cyclic voltammetry of $NiZnFe_2O_5$ NPs/GCE of 0.1 M KCl (pH 7) by varying the concentration of AA at scan rate 0.5 V s^{-1}; B) calibration plot of anodic peak current vs. concentration of AA; C) DPV representation of $NiZnFe_2O_5$ NPs/GCE for AA at a concentrations of 0.2-50.0 µM in (0.1 M KCl, pH 7) at scan rate of 0.5 V/s; D) calibration plot of DPV of current vs. AA concentration*

The electrochemical response of AA on $NiZnFe_2O_5$ NPs/GCE was examined by the DPV technique. The peak current linearly increases with the increasing concentration of AA from 0.2 to 50.0 µM in 0.1 M KCl (pH 7). As shown in Figure 8C, the electrochemical activity of $NiZnFe_2O_5$ NPs/GCE, which improves the electroanalytical function for AA oxidation, caused an increase in the I_{pa} with an increase in the concentration of AA. A linear plot of I_{pa} versus AA concentration is displayed in Figure 8D, similar to the other results from the literature [19,20]. The equivalent equation for the linear regression is Equation (8), which had a range of 0.2 to 50.0 µM.

$$I_{pa} = 8.14601\times10^{-6}\, C_{DPV} + 8.03002\times10^{-5}\ (R^2 = 0.99371) \quad (8)$$

The limit of detection, *i.e.* the lowest concentration of DPV can be determined using Equation (9):

$$\text{LOD} = 3.3\ \sigma/S \quad (9)$$

where σ is the standard deviation of the response and S is the slope of the calibration curve. The limit of detection calculated using Equation (9) gives the value of 1.03897 µM. The $NiZnFe_2O_5$ NPs/GCE electroanalytical potential was contrasted to those of previously released sensors to determine AA. Because $NiZnFe_2O_5$ NPs have a higher surface area, more active sites, and higher catalytic activity, the $NiZnFe_2O_5$ NPs/GCE performs better. Table 2 compares a few different AA electrochemical sensors. Our DPV sensor observes a larger linear dynamic range concentration than the previously published AA sensors. These findings could be explained by a notable rise in the GCE's active surface area when the $NiZnFe_2O_5$ NPs are present [21-29].

Table 2. *Analysing the sensor's performance with other electrochemical sensors*

Modified electrode	Method	Linear range, µM,	LOD, µM	Ref.
CCE/WCNT	DPV	15 to 100	7.71	[21]
GCE/CNO-$NiMoO_4$-$MnWO_4$	DPV	1 to 100	0.33	[22]
GCE/ZnS/rGO/CTAB	Amperometry	50 to 1000	30.00	[23]
GCE/rGO/Au-Pd	DPV	50 to 290	2.83	[24]
SPCE	CV	0 to 10000	1360.00	[25]
CCE/BN	*DPV*	30 to 1000	3.76	[26]
GCE/TiO_2-RuO_2	Amperometry	10 to 1500	1.80	[27]
e-GPE	DPV	20 to 400	2.00	[28]
GCE/MWCNT/CTAB-CO	DPV	5 to 300	1.00	[29]
x$NiZnFe_2O_5$ NPs/GCE	DPV	0.2 to 50.0	1.03897	Present

e-GCE - exfoliated graphite paper electrode, CCE - Ceramic carbon electrode, BN - Boron nitride, GCE- Glassy carbon electrode, BN - Boron nitride, SPCE - Screen-printed carbon electrode

Scheme 1 illustrates the probable electrochemical oxidation pathway of AA at $NiZnFe_2O_5$ NPs/GCE. It is clear that AA is catalytically oxidized into dehydroascorbic acid by removing two electrons.

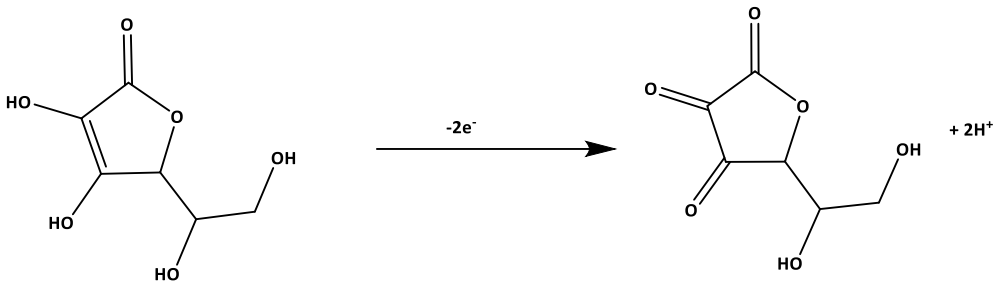

Scheme 1. *Electrochemical oxidation of AA*

Effect of Interference, reproducibility, pH and storage stability studies

CV was used to evaluate the selectivity of the $NiZnFe_2O_5$NPs/GCE sensor on AA in the presence of different biological compounds and certain metals. The CV curves of 2.5 µM AA and threefold

concentrations of different interfering compounds, such as glucose, aspirin, cerium, copper, and molybdenum, are displayed in Figure 9A. Five distinct $NiZnFe_2O_5$ NPs/GCE were tested for repeatability using CV in 2.5 µM AA Figure 9B. A tiny change in the current response magnitude is anticipated for each of the five electrodes. It confirms the five $NiZnFe_2O_5$ NPs/GCE-modified GCE electrodes show good repeatability. The stability of the $NiZnFe_2O_5$ NPs/GCE was tested for about 22 days, as shown in Figure 9C. The CV was taken every 3-day intervals. It showed a small decrease in peak current intensity as good stability with the associated I_{pa} values at 100, 99.9, 98.8, 98.2, 97.99, 97.75 and 96.88 % current height. The current intensity of 96.88 % based on the original value was maintained after 22 days of storage, indicating that the $NiZnFe_2O_5$ NPs/GCE sensor has excellent storage stability. The pH of the analyte significantly influences the peak current and potential. Figure 9D shows the pH dependence of the current peak height. The current increased significantly when the pH increased from 3.0 to 7.0 and gradually decreased from 7.0 to 13.0. It is noted that pH 7.0 is the ideal pH value for an accurate, well-resolved, high-intense signal. The present prominent oxidation peak for AA was observed at pH 7.0. These observations led to using 0.1 M KCl (pH 7) in all electrochemical experiments conducted in this study.

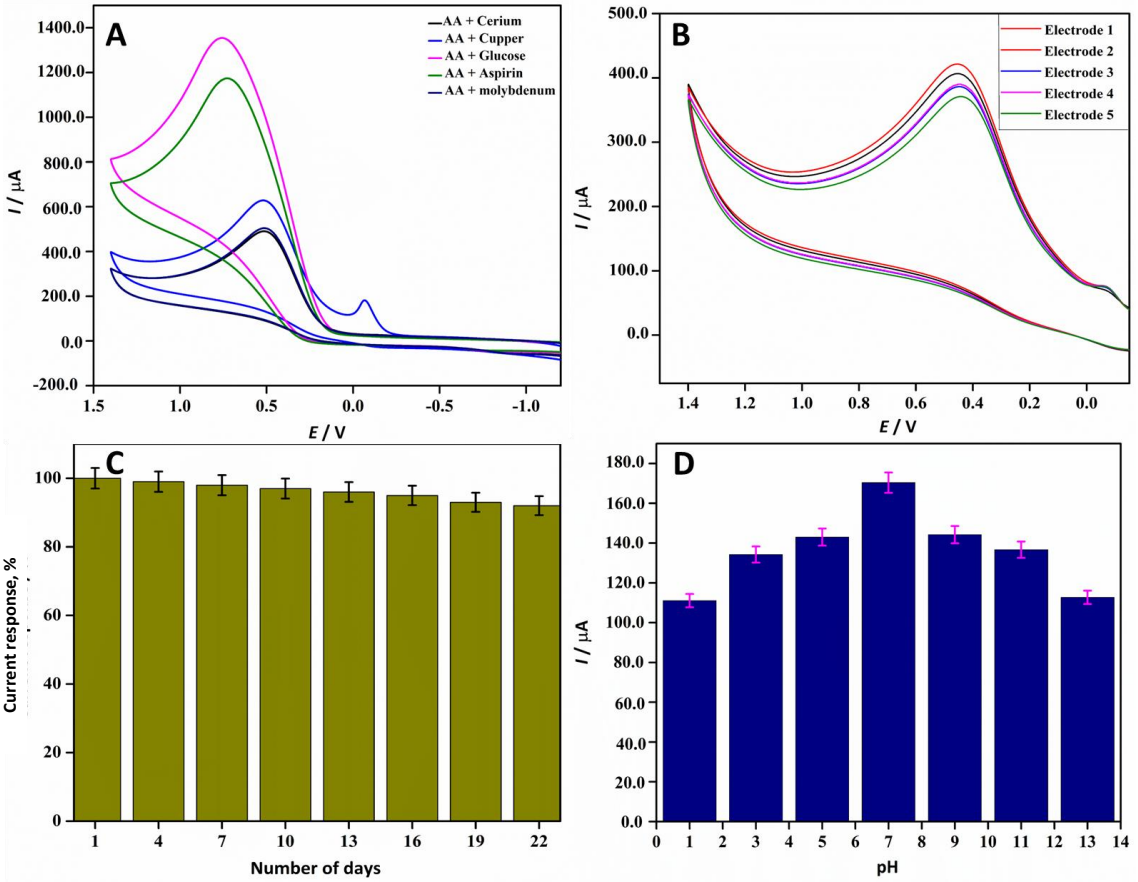

Figure 9. *A) Selectivity of AA (2.5 µM) detection at $NiZnFe_2O_5$ NPs/GCE in 0.1 M KCl, in presence of three-times higher concentrations of denoted interferents; B) repeatability of five separate $NiZnFe_2O_5$ NPs/GCE in 0.1 M KCl and 2.5 µM AA; C) storage stability of $NiZnFe_2O_5$ NPs/GCE for AA detection; D) pH dependence of current peak height of 2.5 µM AA at $NiZnFe_2O_5$ NPs/GCE in 0.1 M KCl*

Real sample analysis

Orange fruit extract and vitamin C tablets were used for real sample analysis. The samples were analysed using a $NiZnFe_2O_5$ NPs/GCE modified electrode. CV evaluated the viability of using the $NiZnFe_2O_5$ NPs/GCE electrochemical sensor for the real-time detection of AA in real samples, including orange fruit and vitamin C tablets. The consistent findings are shown in Figure 10A. Prior

to the study, real samples were taken, and the samples showed no signs of AA [30]. The real samples were then spiked with an identified concentration of AA, and the electrochemical reactions were examined. The CV response and linear plot for orange fruit juice samples containing AA (1, 2, 3, 4, and 5 µM) are displayed in Figure 10B. Similar to this, Figure 10C and Figure 10D show the CV curves of vitamin C tablet samples spiked with AA (1, 2, 3, 4, and 5 µM) together with the matching linear plot. Table 3, which summarises the recovery results of the orange fruit juice and vitamin C tablet, shows that the $NiZnFe_2O_5$ NPs/GCE have a notable recovery for detecting AA in real samples.

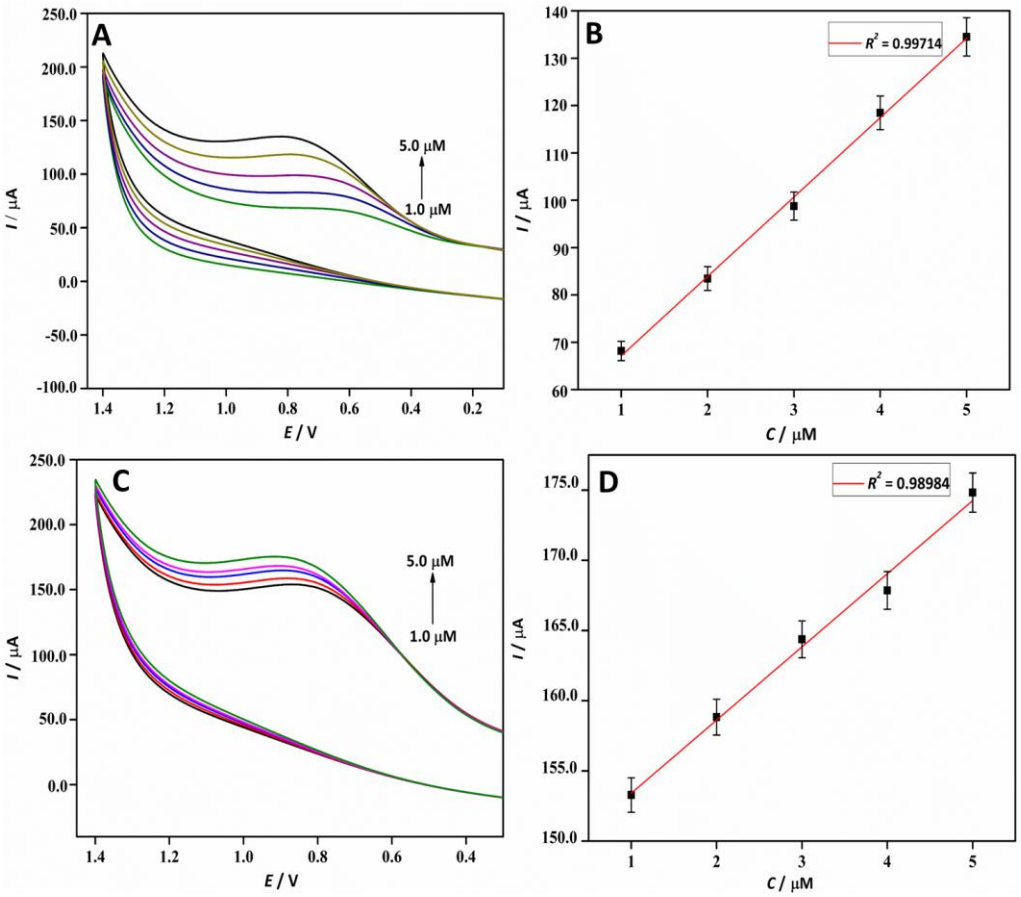

Figure 10. *A) Cyclic voltammetry (0.5 V s^{-1}) of $NiZnFe_2O_5$ NPs/GCE in orange juice with varying concentrations of added AA; B) calibration plot of current* vs. *concentration of AA in orange juice sample; C) CVs (0.5 V s^{-1}) of AA tablet sample with varying concentrations of added AA; D) calibration plot of current* vs. *AA concentration in AA-tablet sample*

Table 3. *Ascorbic acid detection in a variety of real samples using the $NiZnFe_2O_5$ NPs/GCE*

Real sample	Amount, µM		Recovery, %
	Added	Found	
Orange juice	1	1.23	123.00
	2	2.20	110.00
	3	3.19	106.33
	4	4.26	106.50
	5	5.21	104.20
Vitamin C tablet	1	1.34	134.00
	2	2.29	114.50
	3	3.26	108.66
	4	4.31	107.75
	5	5.32	106.40

The linear regression coefficient follows Equations (10) and (11).

$$I_{pa} = 1.67686\ C_{OJ} + 5.03633\times10^{-5}\ (R^2 = 0.99714) \quad (10)$$

$$I_{pa} = 5.21224\times10^{-6}\ C_{AA} + 1.48195\times10^{-4}\ (R^2 = 0.98984) \quad (11)$$

Conclusion

The present studies developed $NiZnFe_2O_5$ NPs using papaya leaf extract to investigate their potential for electrochemical sensing. The $NiZnFe_2O_5$ NPs electrochemical properties were examined by CV, EIS, and DPV. Their characterization was done by utilizing a variety of spectrophotometric methods, including XRD, SEM, EDX, UV-Vis DRS, and DLS. The $NiZnFe_2O_5$ NPs-modified GCE was used to detect AA. The DPV results, notably, showed a broad linear range from 0.2 to 50 µM and a low LOD of 1.03897 µM for AA detection. The suggested sensor also demonstrated excellent repeatability, strong stability, and anti-interfering activity. Moreover, the developed sensor's real-time applicability for calculating the AA content of AA and orange fruit(juice), with results showing notable recovery.

Acknowledgment: *The authors are greatly thankful to Sri Jayachamarajendra College of Engineering (SJCE), JSS Science and Technology University, Mysuru.*

Competing financial interests: *The authors declare no competing financial interest.*

Author Contribution: *G. N. Chandana: Conducted the chemical experiment and tabulated data. S Jeevitha and M.S. Asha: Conducted the chemical experiment. M. B. Shivaswamy: Prepared the manuscript and analysed the characterization data. H.S. Nagendra Prasad: Supervisor and Design, lead the entire project and reviewed the manuscript. M. A. Sangamesha: Performed electrochemical analysis. B.S. Hemanth: Reviewed and improved the quality of the manuscript. B.S. Madhukar: Reviewed the manuscript L Mallesha: Reviewed the manuscript. J G Manjunath: Reviewed the manuscript and improved the quality of the manuscript.*

References

[1] P. G. Jamkhande, N. W. Ghule, A. H. Bamer, M. G. Kalaskar, Metal nanoparticles synthesis: An overview on methods of preparation, advantages and disadvantages, and applications, *Journal of Drug Delivery Science and Technology* **53** (2019) 101174. https://doi.org/10.1016/j.jddst.2019.101174

[2] S. A. Farhan, R. Dadoosh, A. jassim, Evaluation of Phytochemical, Total phenolic and Antioxidant Activity of Carica Papaya Seed for Its Use in Biosynthesis of Gold Nanoparticles, *Egyptian Journal of Chemistry* **64** (2021) 4301-4310. https://doi.org/10.21608/ejchem.2021.63985.3371

[3] G. Kesavan, N. Nataraj, S.-M. Chen, L.-H. Lin, Hydrothermal synthesis of $NiFe_2O_4$ nanoparticles as an efficient electrocatalyst for the electrochemical detection of bisphenol A, *New Journal of Chemistry* **44** (2020) 7698-7707. https://doi.org/10.1039/D0NJ00608D

[4] S. Z. Bas, N. Yuncu, K. Atacan, M. Ozmen, A comparison study of MFe2O4 (M: Ni, Cu, Zn)-reduced graphene oxide nanocomposite for electrochemical detection of bisphenol A, *Electrochimica Acta* **386** (2021) 138519. https://doi.org/10.1016/j.electacta.2021.138519

[5] M. Derakhshi, T. Jamali, M. Elyasi, M. Bijad, R. Sadeghi, A. Kamali, K. Niazazari, M. R. Shahmiri, A. Bahari, S. Mokhtari, Synthesis and Characterization of NiO Nanoparticle as a High Sensitive Voltammetric Sensor for Vitamin C Determination in Food Samples, *Journal of the Serbian Chemical Society* **8** (2013) 8252-8263. https://doi.org/10.1016/S1452-3981(23)12884-7

[6] T. Peik-See, A. Pandikumar, H. Nay-Ming, L. Hong-Ngee, Y. Sulaiman, Simultaneous Electrochemical Detection of Dopamine and Ascorbic Acid Using an Iron Oxide/Reduced Graphene Oxide Modified Glassy Carbon Electrode, *Sensors* **14** (2014) 15227-15243. https://doi.org/10.3390/s140815227

[7] M. Dosedel, E. Jirkovsky, K. Macakova, L. Krcmova, L. Javorska, J. Pourova, L. Mercolini, F. Remiao, L. Novakova, P. Mladenka, Vitamin C-Sources, Physiological Role, Kinetics, Deficiency, Use, Toxicity, and Determination, *Nutrients* **13** (2021) 615. https://doi.org/10.3390/nu13020615.

[8] S. Jeevitha, H. S. Nagendra Prasad, M. B. Shivaswamy, M. S. Asha, S. R. Arjun, G. N. Chandana, M. A. Sangamesha, B. S. Madhukar, B. S. Hemanth, Sabu Thomas, Facile green preparation of ZnFe2O4 nanoparticles using papaya leaf extract for electrochemical detection of acetaminophen in Zerodol P and Dolo drops, *Ionics* **30** (2024) 8617-8630. https://doi.org/10.1007/s11581-024-05879-6

[9] P. Sivakumar, R. Ramesh, A. Ramanand, S. Ponnusamy, C. Muthamizhchelvan, Preparation and properties of nickel ferrite (NiFe2O4) nanoparticles via sol-gel auto-combustion method, *Materials Research Bulletin* **46** (2011) 2204-2207. https://doi.org/10.1016/j.materresbull.2011.09.010

[10] H. M. Zaid, M. Adil, K. C. Lee, Structural and morphological evolution of metal oxide nanoparticles synthesised via sol-gel auto-combustion, *International Journal of Nanotechnology* **14** (2017) 284. https://doi.org/10.1504/IJNT.2017.082478

[11] H. R. Ebrahimi, M. Parish, G. R. Amiri, B. Bahraminejad, S. Fatahian, Synthesis, characterization and gas sensitivity investigation of $Ni_{0.5}Zn_{0.5}Fe_2O_4$ nanoparticles, *Journal of Magnetism and Magnetic Materials* **414** (2016) 55-58. https://doi.org/10.1016/j.jmmm.2016.04.043

[12] S. Alaei, M. Haghighi, J. Toghiani, B. Rahmani Vahid, Magnetic and reusable MgO/MgFe2O4 nanocatalyst for biodiesel production from sunflower oil: Influence of fuel ratio in combustion synthesis on catalytic properties and performance, *Industrial Crops and Products* **117** (2018) 322-332. https://doi.org/10.1016/j.indcrop.2018.03.015

[13] S. Landi, I. R. Segundo, E. Freitas, M. Vasilevskiy, J. Carneiro, C. J. Tavares, Use and misuse of the Kubelka-Munk function to obtain the band gap energy from diffuse reflectance measurements, *Solid State Communications* **341** (2022) 114573. https://doi.org/10.1016/j.ssc.2021.114573

[14] B. S. Hemanth, M. J. Deviprasad, M. B. Shivaswamy, H. S. Nagendra Prasad, S. Sumathi, R. Aswathy, M. A. Sangamesha, A. P. Ananda, H. S. Jayanth, T. N. Lohith, Synthesis of citral-tryptamine fused selenium nanospheres (CT@SeNP's) and exploration of their anticancer, antibacterial, and electrochemical sensor applications, *Journal of Molecular Structure* **1310** (2024) 138240. https://doi.org/10.1016/j.molstruc.2024.138240

[15] M. P. Ujwal, S. R. Yashas, H. P. Shivaraju, N. Kumara Swamy, Gadolinium ortho-ferrite interfaced polyaniline: Bi-functional catalyst for electrochemical detection and photocatalytic degradation of acetaminophen, *Surfaces and Interfaces* **30** (2022) 101878. https://doi.org/10.1016/j.surfin.2022.101878

[16] M. K. Manju, J.G. Manjunatha, K. Bhimaraya, S. A. Aldossari, S. Mohammad, M. Sillanpää, Simultaneous electrochemical detection of hydroquinone and catechol using a carbon nanotube paste electrode modified with electrochemically polymerized L-alanine, *Chemical Papers* **78** (2024) 8019-8030. https://doi.org/10.1007/s11696-024-03652-7

[17] A. A.Rashak, F. F. Karam, Preparation of graphene oxide and multi-walled carbon nanotubes, and they are used to modify the glassy carbon electrode for sensing Enalapril Maleate, *Results in Chemistry* **8** (2024) 101597. doi.org/10.1016/j.rechem.2024.101597

[18] R. Santhosh Kumar, K. Govindan, S. Ramakrishnan, A. R. Kim, J.-S. Kim, D. J. Yoo, Fe3O4 nanorods decorated on polypyrrole/reduced graphene oxide for electrochemical detection of dopamine and photocatalytic degradation of acetaminophen, *Applied Surface Science* **556** (2021) 149765. https://doi.org/10.1016/j.apsusc.2021.149765

[19] M. B. Shivaswamy, P. Karthikdev, B. S. Madhukar, B. S. Hemanth, M. J. Deviprasad, R. Kavya, M. A. Sangamesha, A. P. Anand, H. P. Spoorthy, H. S. Nagendra Prasad, Silver fused multifunctional CeIn2O5 nanoparticle: Photocatalytic, antibacterial and electrochemical sensor studies, *Chemistry of Inorganic Materials* **2** (2024) 100042. https://doi.org/10.1016/j.cinorg.2024.100042

[20] S. Kubendhiran, R. Sakthivel, S.-M. Chen, R. Anbazhagan, H.-C. Tsai, A novel design and synthesis of ruthenium sulfide decorated activated graphite nanocomposite for the electrochemical determination of antipsychotic drug chlorpromazine, *Composites Part B: Engineering* **168** (2019) 282-290. https://doi.org/10.1016/j.compositesb.2018.12.082

[21] B. Habibi, M. H. Pournaghi-Azar, Simultaneous determination of ascorbic acid, dopamine and uric acid by use of a MWCNT modified carbon-ceramic electrode and differential pulse voltammetry, *Electrochimica Acta* **55** (2010) 5492-5498. https://doi.org/10.1016/j.electacta.2010.04.052

[22] M. Saleh Mohammadnia, E. Marzi Khosrowshahi, E. Naghian, A. Homayoun Keihan, E. Sohouli, M. E. Plonska-Brzezinska, A. Sobhani-Nasab, M. Rahimi-Nasrabadi, F. Ahmadi, Application of carbon nanoonion-NiMoO4-MnWO4 nanocomposite for modification of glassy carbon electrode: Electrochemical determination of ascorbic acid, *Microchemical Journal* **159** (2020) 105470. https://doi.org/10.1016/j.microc.2020.105470

[23] Y. J. Yang, One-pot synthesis of reduced graphene oxide/zinc sulfide nanocomposite at room temperature for simultaneous determination of ascorbic acid, dopamine and uric acid, *Sensors and Actuators B* **221** (2015) 750-759. https://doi.org/10.1016/j.snb.2015.06.150.

[24] L. Zhang, G. Wang, D. Wu, C. Xiong, L. Zheng, Y. Ding, H. Lu, G. Zhang, L. Qiu, Highly selective and sensitive sensor based on an organic electrochemical transistor for the detection of ascorbic acid, *Biosensors and Bioelectronics* **100** (2018) 235-241. https://doi.org/10.1016/j.bios.2017.09.006

[25] J. K. Jadav, V. V. Umrania, K. J. Rathod, B. A. Golakiya, Development of silver/carbon screen-printed electrode for rapid determination of vitamin C from fruit juices, *LWT - Food Science and Technology* **88** (2018) 152-158. https://doi.org/10.1016/j.lwt.2017.10.005

[26] M. S. Raghu, L. Parashuram, K. Y. Kumar, B. P. Prasanna, S. Rao, P. Krishnaiah, K. N. Prashanth, C. B. P. Kumar, H. Alrobei, Facile green synthesis of boroncarbonitride using orange peel; Its application in high-performance supercapacitors and detection of levodopa in real samples, *Materials Today Communications* **24** (2020) 101033. https://doi.org/10.1016/j.mtcomm.2020.101033

[27] P. Shakkthivel, S.-M. Chen, Simultaneous determination of ascorbic acid and dopamine in the presence of uric acid on ruthenium oxide modified electrode, *Biosensors and Bioelectronics* **22** (2007) 1680-1687. https://doi.org/10.1016/j.bios.2006.07.026

[28] A. Murali, Y. P. Lan, P. K. Sarswat, M. L. Free, Synthesis of CeO2/reduced graphene oxide nanocomposite for electrochemical determination of ascorbic acid and dopamine and for photocatalytic applications, *Materials Today Chemistry* **12** (2019) 222-232. https://doi.org/10.1016/j.mtchem.2019.02.001

[29] B. Kaur, T. Pandiyan, B. Satpati, R. Srivastava, Simultaneous and sensitive determination of ascorbic acid, dopamine, uric acid, and tryptophan with silver nanoparticles-decorated reduced graphene oxide modified electrode, *Colloids and Surfaces B: Biointerfaces* **111** (2013) 97-106. https://doi.org/10.1016/j.colsurfb.2013.05.023

[30] V. Vinothkumar, R. Sakthivel, S.-M. Chen, T. H. Kim, M. Abinaya, S. Kubendhiran, G. Gopu, Nanoarchitectured nickel phosphate integrated with graphene oxide for the toxicant diphenylamine detection in food samples, *Journal of Food Composition and Analysis* **111** (2022) 104628. https://doi.org/10.1016/j.jfca.2022.104628